Rodríguez-Sánchez, M. R., Sánchez-González, A. & Santana, D. (2018). Feasibility study of a new concept of solar external receiver: Variable velocity receiver. *Applied Thermal Engineering*, 128, pp. 335–344.

DOI: 10.1016/j.applthermaleng.2017.08.173

Feasibility study of a new concept of solar external receiver: variable velocity receiver

M.R. Rodríguez-Sánchez[1, a)], A. Sánchez-González[1], D. Santana[1]

[1] *Energy Systems Engineering Group (ISE). Department of Thermal and Fluids Engineering from Universidad Carlos III de Madrid. Av. Universidad 30, Leganés, 28911 Madrid (Spain).*

a) Corresponding author: mrrsanch@ing.uc3m.es

Abstract

The deployment of new solar power tower plants mainly depends on becoming cost-competitive with traditional forms of electricity generation. The solar field represents around 40% of the solar power tower investment cost, thus the cost reduction of such subsystems is mandatory to achieve that goal. This reduction could be done by increasing the solar flux intercepted by the receiver, which would increase the peak flux. Therefore, new concepts of solar receivers are required to accommodate such high peak flux.

The proposed receiver, which withstands high peak flux, consists on a Traditional External Tubular Receiver (TETR) equipped with valves that allow the division of each panel of the receiver in two independent panels, increasing the velocity of the heat transfer fluid in specific zones of the receiver. This receiver configuration, named *Variable Velocity Receiver* (VVR), avoids tube overheating. Moreover, this novel receiver allows more concentrated aiming strategies, which increases the optical efficiency of the solar field and permits to reduce the number of heliostats in the field. Given a specific generation capacity, the size of the solar field required by a VVR is 12.5% smaller in comparison to a TETR.

Such efficiency improvement has a negligible effect in tube mechanical stresses; even though pressure drop and parasitic consumption of the power plant increase. This new receiver

configuration also gains hours of operation, even in winter: in hours with low solar irradiance all the panels can be split in two, increasing the number of passes and the velocity of the heat transfer fluid and accomplishing the transition from laminar to turbulent regime. Therefore, this receiver is able to reduce the levelized cost of energy.

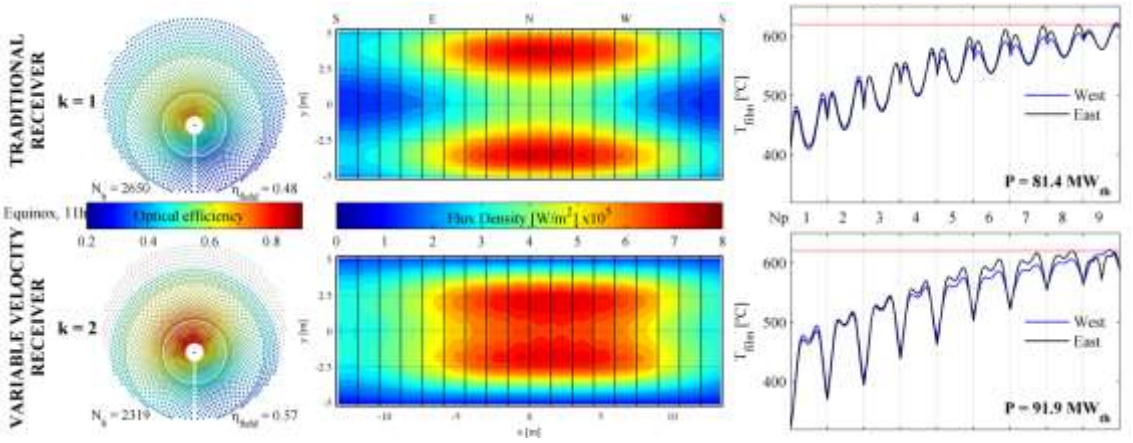

Key words: Solar power tower; External tubular receiver; Variable velocity; Generation capacity; Solar field.

1. Introduction

Solar power tower (SPT) systems use numerous sun-tracking mirrors to concentrate sunlight onto a receiver, situated at the top of a tower. Solar energy is collected in the receiver using a heat transfer fluid (HTF) which is then used to transfer the energy to a thermodynamic power cycle. Then, SPT consists of two main subsystems: one that collects solar energy and converts it into heat, and another that converts thermal energy into electricity. This study is devoted to the improvement of the first part of the SPT, which includes the solar field and the central receiver.

The main challenge for SPT is to increase the lifetime of the highly irradiated receiver, whilst ensuring a cost effective design. If the reflected solar radiation is concentrated on the receiver equator, high solar concentration ratio and high optical efficiencies of the field are achieved. It increases the generation capacity of the SPT or, alternatively, reduces the required size of the

solar field for a given constant generation capacity, being crucial to economic feasibility of the SPT. However, high solar concentration produces overheating of the absorber material, accelerating the risk of failure by stress corrosion cracking. Hence, a multi-level aiming strategy is required to reduce the wall temperature, at the expense of reducing the efficiency of the SPT and, ultimately, its economic feasibility. Moreover, scattered aiming strategies require permanent control of the heliostats position, making SPT operation more complex.

Numerous researches focused their studies in optimizing the design of the receiver and the solar field to reduce the levelized cost of electricity. With respect to the solar field, Ruiz et al. [1] proposed a variable geometry central receiver facility, in which the solar field rotates around the tower axis, following the sun azimuth along the day and reducing the number of heliostats required. Related to the thermal storage, Hübner et al. [2] proposed a combined sensible molten salt thermal energy storage plus an alkali salt latent heat thermal energy storage, in order to increase the power generated by the SPT. Regarding the absorber materials, Neises et al. [3] tested a new receiver material that could withstand high solar flux and temperature, while Prasad et al. [4] designed single, double and triple layer absorber tandems to control the chemical oxidation and to improve the optical properties of the absorber material, the problem of this material is that cannot withstand high temperatures. Related to the HTF, Boerema et al. [5] compared the advantages of using different HTF and Rodríguez-Sánchez et al. [6] optimized the flow pattern of the external receivers which enlarges the useful lifetime of the receivers. On the other hand, several authors proposed new concepts of solar receivers, among them Garbrecht [7] studied a receiver geometry based on hexagonal pyramid-shaped elements, Rodríguez-Sánchez et al. [8] analysed an external receiver in which the tubes were replaced by bayonet tubes, Boerema et al. [9] investigated new designs using different tube diameters in each panel, Turner and Sansom [10] studied a low-cost modular receiver that consists on a volumetric cavity receiver formed by tubular structures, and Yang et al. [11] introduced a high temperature two-phase flat heat pipe

receiver, with sodium as HTF, which homogenises the temperature in cavity systems. However, none of these designs can optimize the receiver design for the whole operational range in a SPT, which depends on sun position. Thus, SPT does not take advantage of the maximum energy available and tube overheating still takes place.

A new concept of external tubular receiver, named *Variable Velocity Receiver* (VVR), is introduced and analyzed from the point of view of mechanical and thermal limitations, as well as cost effectiveness. VVR can increase/reduce the velocity of the HTF in specific zones of the receiver thanks to a valve system; therefore it uses the advantages of a receiver with high number of panels without an elevated parasitic consumption. VVR can be adapted to the evolution of concentrated solar flux along the day, reducing the control load associated to the solar field. Moreover, the possibility of increasing HTF velocity in selected parts of the receiver, reduces tube overheating problems and allows higher concentration ratios in the receiver, reducing spillage losses [12]. Thus, the use of VVR reduces the number of heliostats required in the field and, ultimately, the levelized cost of electricity.

This paper describes the main characteristics of VVRs and presents their main differences with respect to Traditional External Tubular Receivers (TETRs). Firstly, the operation of the VVR has been described, as well as the optical and thermal model employed to characterize the instantaneous behaviour of the field and the receiver. Secondly, the configuration of the VVR has been optimized for a given generation capacity during the Spring Equinox. This optimization was based on the hourly thermal, mechanical and hydraulic behaviour. Finally, TETRs and VVRs of the same generation capacity have been compared.

2. Receiver configuration

In this study, the proposed receiver configuration is an external tubular receiver, based on Gemasolar power plant, located in Seville at 37.56^{o} North latitude. The receiver is a 360^{o} cylindrical external receiver of 10.5 m in height, *H*, and 8.5 m in diameter mounted on a 120 m

high tower. The receiver is formed by 18 panels of 1.48 m width; in each panel there is one inlet header and one outlet header, located in opposite sides (top and bottom). The headers are connected by 60 vertical tubes of Alloy 800H coated with black Pyromark. The external diameter of the tubes, d_o, is 0.0221 m and the thickness, *th*, 0.0012 m. In the rear part of the tubes a refractory wall reduces the thermal losses.

The HTF flowing by the receiver is solar salt (60% $NaNO_3$ - 40% KNO_3). This salt is heated from 290 ^oC to 565 ^oC. The inlet of the receiver is located at the two northern panels and the molten salt moves towards the southern panels in two different paths (East and West paths). The salt flows in parallel (i.e. same direction) through all the tubes of a panel, and in series from one panel to the following, as can be seen in Figure 1.a. The design thermal power absorbed by the salt in the receiver is 120 MW_{th}.

Using the same tube diameter, d_o, receivers with high number of panels, N_p, reduce the wall temperature of the tubes; however this kind of receivers has high pressure drop, which in turn increases the parasitic consumption of the SPT [13]. To take advantage of a receiver with high number of panels without its disadvantages, the concept of variable velocity receiver arises.

The VVR consists on a receiver with the same characteristics as the TETR. Additionally, each header is divided in two independent headers as the receiver proposed by Das et al. [14], called Alstom Receiver (AR). The new receiver has two inlets and two outlets headers per panel; each pair of headers connects half the number of tubes than the original panel of the TETR (30 tubes). Despite of the division the behaviour of AR is equivalent to the TETR since the new pair of panels works in parallel, keeping constant the number of passes of the receiver, see Figure 1.b. The novelty of the VVR with respect to the AR lies in the valve system installed between the headers of the same side (top or bottom). The valve system can keep the panel working as the AR, as shown Figure 1.c (pairs of panels working in parallel, keeping constant the number of passes of the receiver), or can divide the panels in two independent ones

(working in series, and increasing the number of passes of the receiver). In order to improve the receiver behaviour, such divisions are only performed in those panels in which the wall temperature overpasses the safe operational limit, see Figure 1.d.

When all the pairs of new panels work in parallel the number of passes and the HTF velocity is the same than for Alstom and TETR. When all the pairs of new panels work in series the number of passes and the HTF velocity rate doubles the original one. This configuration decreases the wall temperature at the expense of increasing the pressure drop. Nevertheless, when the pairs of new panels work in any combination of both, series and parallel, the HTF velocity varies from one panel to the next, diminishing the maximum temperatures while the pressure drop is moderately kept down, although it will be higher than in the TETR.

Therefore, depending on the solar flux distribution, in the VVR different panels can be divided and combined. To distinguish the different combinations of VVRs each panel has been denoted by an arrow, whose colour depends on the direction of the flow, where ↓ indicates the descending direction and ↑ the ascending direction. To obtain a direct equivalence between TETR and VVR, the TETR configuration is named as the AR configuration. Then, for the three receivers shown in Figures 1.a, 1.b and 1.c the configuration would be: ↓↓↑↑↓↓↑↑, consisting of 4 passes and for Figure 1.d the configuration would be: ↓↓↑↑↓↑↓↑, consisting of 6 passes.

Rodríguez-Sánchez et al. [12] carried out a thermodynamic study of a VVR with three divisions per panel, obtaining an extreme, not feasible, pressure drop. Thus, although it would be possible to divide each original panel in more than two passes, it has been disregarded.

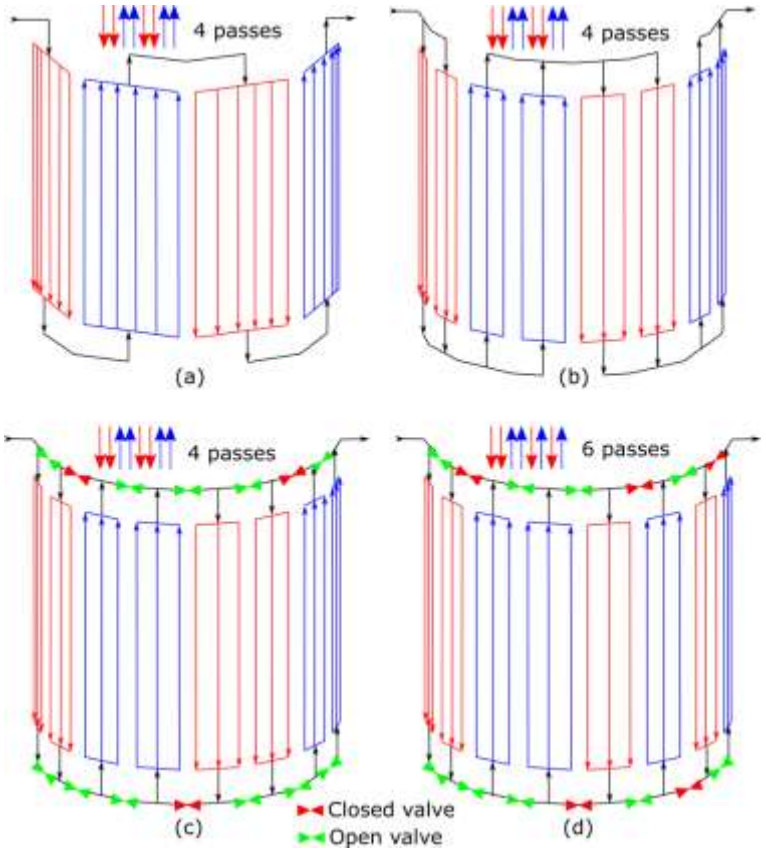

Figure 1 - Schematic of the flow path configuration of (a) a TETR (b) an AR [14] (c) a VVR working as an AR (d) a VVR with several pairs of panels working in parallel (1-2, 3-4) and several in series (5-6, 7-8).

3. Field-receiver model

The solar field of Gemasolar follows a cornfield layout in the inner zone and a radial staggered in the two external zones. The position of the $N_h = 2650$ square heliostats in the layout, each one of 10.95 m side, was obtained from scaled aerial images of the SPT, see Figure 2.

The model developed by Sánchez-González and Santana [15] has been used to obtain the incident solar flux on the receiver, ϕ_{inc}, according to Equation 1, where: *DNI* is the direct normal irradiance, obtained from the clear sky model by Hottel [16]; and *C* corresponds to the concentration ratio of flux density calculated with the projection method [15]. The flux distribution on the image plane is based on a circular Gaussian effective error, γ_e, resulting

from the convolution of sunshape (γ_{sun} = 2.51 mrad) and mirror slope (γ_{slp} = 2.1 mrad), as defined Equation 2 [17].

$$\phi_{inc} = \sum_{i=1}^{Nh} C_i \cdot DNI \tag{1}$$

$$\gamma_e = \sqrt{\gamma_{sun}^2 + 2\left(1 + \cos \varpi_h\right)} \tag{2}$$

The heliostat efficiency, η_h, is computed using Equation 3 where: ρ represents the reflectivity of the mirrors, which has been assumed constant and equal to 0.836; ω_h corresponds to the angle between the sun and the heliostats normal; f_{atm} is the atmospheric attenuation factor [18]; f_{sb} is the shadowing and blocking factor [19]; and f_{sp} is the spillage factor [15]. The overall heliostat field efficiency is thus the average: $\eta_{field} = \sum \eta_h / N_h$.

$$\eta_h = \rho \cos(\omega_h) f_{atm} f_{sb} f_{sp} \tag{3}$$

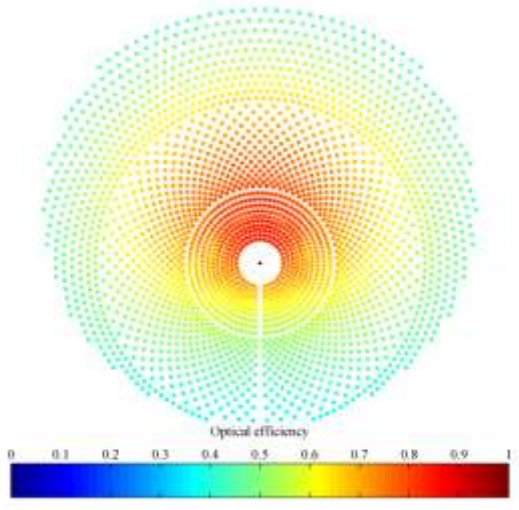

Figure 2- Solar field layout and heliostat efficiencies at Spring Equinox noon with an equatorial aiming strategy.

166 To characterize the aiming strategy it was used the non-dimensional parameter, *k*, which has
167 been called aiming factor and indicates the probability distribution. Symmetric flux maps about
168 the receiver equator with controlled spillage losses are gained through the aiming factor
169 approach [15]. By analogy with the circular normal distribution, 68%, 95% and 99.7% of the
170 total flux is within the cone of aperture angles γ_e, $2\gamma_e$ and $3\gamma_e$, respectively. Where *k* is the
171 factor multiplying the effective error. Heliostat target points are vertically shifted so that the
172 beam circumference is tangent to either the upper or the lower receiver edge. The radius of
173 the incident beam on the receiver (BR_k) is dependent on the aiming factor, according to
174 Equation 4, where *SLR* stands for the distance from the heliostat to the receiver and ε_t is the
175 elevation angle of the target vector.

176 $$BR_k = k\frac{SLR\cdot\gamma_e}{\cos(\varepsilon_t)} \quad (4)$$

177 Therefore, an equatorial aiming strategy (*k* ~ 3) minimizes spillage losses of the field but may
178 cause receiver overheating. A scattered aiming strategy (lower *k* values) reduces the optical
179 efficiency of the field but also reduces the risk of damage of the receivers.

180 To simulate the thermal, mechanical and hydrodynamic behaviour of the receiver, the model
181 developed by Rodríguez-Sánchez et al. [13] has been employed. The main characteristics of
182 this model are that it considers circumferential variations of the temperature, that only
183 analyses a representative tube per panel, and that the properties of the HTF and the tube
184 material are dependent of the temperature [20]. This simplified model was validated with the
185 experimental data of solar flux published by Pacheco [21] in [22]. Moreover, it produces similar
186 results than CFD models with lower computational cost [23].

187 Given the inlet and outlet set point temperatures of the salt, an initial estimation of the wall
188 temperature has been established [24]. After several iterations, described in Figure 3, the

189 model calculates the heat losses by radiation, ϕ_0, and the flux density absorbed by the HTF,

190 ϕ_{abs}, the efficiency of the receiver, η_{rec}, the bulk temperature of the salt, T_{salt}, the wall

191 temperature of the tubes, T_{wall}, and the film temperature, T_{film}, as shown Equations from 5

192 to 9. Where, film temperature is defined as the temperature of the salt in a thin layer close to

193 the tube wall responsible of the tube corrosion. In this study, it has been defined as the

194 temperature of the internal face of the tubes.

195 $$z = 1,...,N_z;\ \ \theta = 1,...,N_\theta;\ \ 0 = ambient;\ \ N_\theta + 1 = refractory\ wall$$

196
$$\begin{aligned}&\left[\frac{\delta_{m,0}}{\varepsilon_0}-\left(\frac{1}{\varepsilon_0}-1\right)F_{m,0}(\theta)\right]\frac{\phi_0(z)}{\sigma_B}+\sum_{j=1}^{N_\theta}\left[\frac{\delta_{m,\mathrm{j}}}{\varepsilon_j(z,\theta)}-\left(\frac{1}{\varepsilon_j(z,\theta)}-1\right)F_{m,j}(\theta)\right]\frac{\phi_0(z,\theta)}{\sigma_B}\\&-\left[\delta_{m,N_\theta+1}-F_{m,N_\theta+1}(\theta)\right]T^4_{N_\theta+1}(z)=\left[\delta_{m,0}-F_{m,0}(\theta)\right]T_0^4+\sum_{j=1}^{N_\theta}\left[\delta_{m,\mathrm{j}}-F_{m,j}(\theta)\right]T_j^4(z,\theta)\\&-\left[\frac{\delta_{m,N_\theta+1}}{\varepsilon_{N_\theta+1}(z)}-\left(\frac{1}{\varepsilon_{N_\theta+1}(z,\theta)}-1\right)F_{m,N_\theta+1}(\theta)\right]\frac{\phi_{abs}(z,\theta)}{\sigma_B}-F_{m,0}(\theta)\frac{\phi_{inc}(z)}{\sigma_B}\alpha_t\end{aligned} \quad (5)$$

197
$$\eta_{rec}=\frac{\phi_{abs}}{\phi_{inc}} \quad (6)$$

198
$$T_{salt}(z)=\mathrm{T}_{\mathrm{salt}}(0)+\frac{z}{\dot{m}_{salt}c}\sum_{1}^{N_\theta}\phi_{abs}(z,\theta)pr(\theta) \quad (7)$$

199
$$\mathrm{T}_{\mathrm{wall}}(z,\theta)=T_{salt}(z)+\frac{\phi_{abs}(z,\theta)}{U(z)} \quad (8)$$

200
$$T_{film}(z,\theta)=T_{wall}(z,\theta)-\frac{1}{2}\phi_{abs}(z,\theta)\frac{d_o\ln(d_o/d_i)}{k_t(z,\theta)} \quad (9)$$

201 σ_B corresponds to the Boltzman constant and α_t to the absorptivity of the tubes in the visible

202 spectrum. F represents the view factors of the problem and δ the Kronecker's delta. ε

depicts the emissivity of the different elements in the infrared spectrum, d_i the internal diameter of the tubes, c the specific heat of the salt, pr the tube perimeter, U the global heat transfer coefficient of each tube arc, k_t the thermal conductivity coefficient of the tubes, h the convective coefficient and R_{foul} the fouling resistance of the tubes, whose value has been assumed of 8.8 10^{-5} m^2K/W.

Once the thermal behaviour has been defined, it is possible to calculate the mechanical stresses of the tubes, σ, and the total pressure drop in the receiver, Δp, see Equations 10 and 11. Where: E corresponds to the Young's modulus, α to the expansion coefficient and ν to the Poisson coefficient, and p_i to the maximum inner pressure. Besides, f represents the Darcy's coefficient, φ the density of the salt, S the cross section area of the tubes, Re the Reynolds number, R the radius of the elbow, and A is a coefficient that depends on the elbow angle [25]. Flores et al. [26] and Marugan et al. [27] pointed that Equation 10 is only valid with large Biot number, as it is the case of the analysed receivers. To calculate the pressure drop it has been assumed that each tube has three elbows, one with an angle of π/3 rad and two with angles of 2π/3 rad. Moreover, each header has an expansion or a contraction together with two extra elbows of π/2 rad.

$$\sigma_{\max} \simeq \frac{E(z)\alpha(z)}{2(1-\nu(z))k_t(z)}\phi_{abs}(\mathrm{z})\,\mathrm{th}+\frac{p_i(z)d_i^2}{d_o^2-d_i^2}\left(1+\frac{d_o^2}{d_i^2}\right) \quad (10)$$

$$\Delta p=\sum_{straight} f\frac{H}{d_i}\frac{\dot{m}_{salt}^2}{2\varphi S^2}+\sum_{\exp/con} K\frac{\dot{m}_{salt}^2}{2\varphi S^2}+\sum_{elbow}\left[\left(1.3-0.29\ln\frac{\mathrm{Re}}{10^5}\right)0.21A\left(\frac{R}{d_i}\right)^{-0.25}\right]\frac{\dot{m}_{salt}^2}{2\varphi S^2} \quad (11)$$

The value of some of the parameters described are shown in Table 1; the expressions to calculate the rest of parameters can be found in ASME [28] and Zavoico [20].

223 Table 1 – Valour assumed for the different variables

Variable	Value	Variable	Value
α_t **[-]**	0.93	K [-]	0.9 (exp.) & 0.4 (con.)
ε_0 **[-]**	0.955	R [m]	0.13
$\varepsilon_{N_\theta+1}$ **[-]**	0.2	A [-]	0.78 & 1 & 1.17
S **[m²]**	1.22 x 10^{-3}	T_{amb} [ºC]	25

224

225 The model also included the limits of operation that must be fulfilled by the receivers. To avoid
226 fatigue and cracking the mechanical stresses must be lower than 33% of the Ultimate Tensile
227 Strength (*UTS*) [28]. The film temperature must be below the limit that enhances tube
228 corrosion; for Alloy 800H that limit corresponds to a temperature of 620 ºC [29]. Besides, it is
229 recommended to keep down the pressure drop in order to avoid increasing the parasitic
230 consumption of the SPT.

231 **4. Results**

232 In this section the most important thermal, mechanical and hydrodynamic factors for the
233 optimal operation of a VVR, with up to two divisions per panel, have been presented and
234 compared with the TETR. It is understood for optimal operation the one that fulfils the limits of
235 operation of the receiver with the maximum field-receiver efficiency possible, $\eta_{field}\eta_{rec}$.

236 The design day of the SPT is the Spring Equinox. As far from the solar noon the behaviour of
237 both flow paths become different, they have been independently analysed. However, due to
238 symmetry with respect to the solar noon only the morning hours were analysed.

239 In the following subsections firstly, it has been explained how to calculate the field layout of
240 the VVR of 120 MW_{th} starting from a traditional SPT layout, as well as how to select the
241 maximum allowable aiming factor. Secondly, a thermal comparison between the TETR and the

VVR has been carried out. And finally, it has been paid attention to the mechanical and hydrodynamic behaviour of both receivers.

4.1. Constant generation capacity

As the VVR admits higher concentration ratios than the TETR, the generation capacity of the new SPT increases if the heliostat field layout is kept. The goal of using the VVR is the design of new SPTs with a given generation capacity, i.e. 120 MW_{th}. Therefore, the new SPT requires less number of heliostats than a traditional SPT. It cuts down the investment cost of the SPT, and moves the operational control to the receiver instead of to the solar field, simplifying the plant operation.

To solve the desirable operating conditions of the TETR the maximum feasible aiming factor has been selected. If the mechanical and thermodynamic restrictions are fulfilled the optimum has been found, otherwise the aiming factor has to be diminished, see Figure 3. To optimize the VVR the procedure is the same; but before decreasing the aiming factor, the panels that overpass the restrictions are divided in two independent panels working in series (i.e. two passes). If restrictions are fulfilled by dividing the panels, the optimum has been found, otherwise the aiming factor must be reduced, see Figure 3. Note that in the VVR, the valve systems installed in both flow paths of the receiver are independent between them; therefore each flow path can operate with different number of passes.

The previous procedure does not consider the generation capacity of the SPT. To determine the total number of heliostats that can be eliminated, it is necessary to analyse the annual power produced by the SPT. However, to simplify the analysis the thermal energy absorbed by the new receiver has been equalled to the energy absorbed by the TETR during the Spring Equinox plus the increment of energy consumption in the molten salt pumps. If even so the VVR absorbs more net thermal energy, the solar field should be diminished.

The removed heliostats would be the less efficient, which correspond to those located at the last rows of the field. Moreover, eliminating heliostats placed in the northern part of the field it is possible to reduce the maximum mechanical stresses, which are located at the first panels of each path. Note, that this work studies the feasibility of the VVR, but the optimization of the solar field is beyond the scope of this paper. Then, there would be multiple options to reduce the number of heliostats in the field, e.g. optimizing the aiming strategy as the proposed in [30].

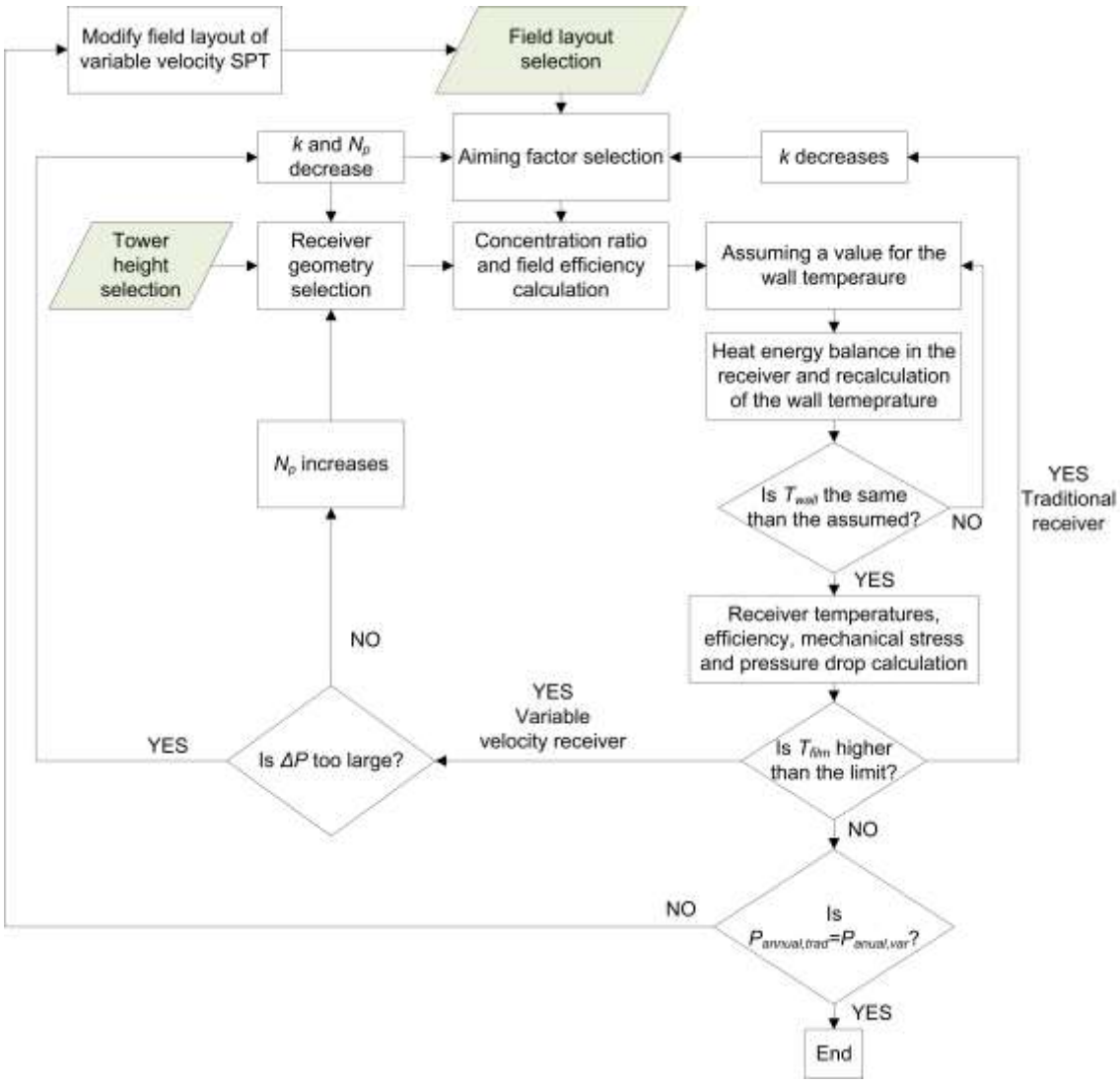

Figure 3- Flow chart of the field-receiver simulation

After the analysis, the solar field obtained for the VVR of 120 MW_{th} consists on the original field without the last six northern rows, see Figure 4. It means 331 less heliostats than in the original layout, namely a field reduction of 12.5%. Assuming a cost of the heliostat of 126 $\$/m^2$ [31], it supposes a capital saving of 4.82 M$ or a 5% of the total investment cost of the SPT. Note that this value does not correspond to the net saving of the new SPT, due to the extra cost of the valves and control system of the VVR.

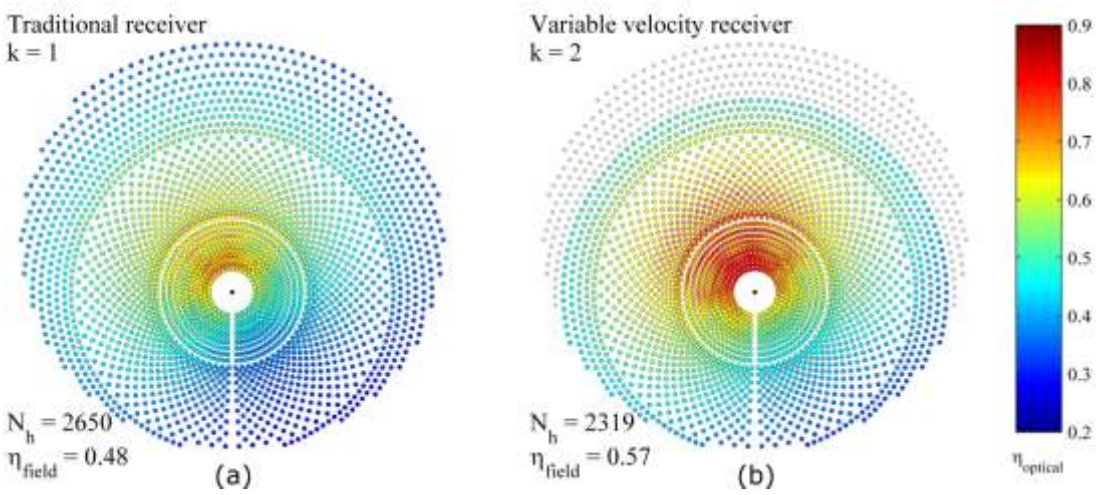

Figure 4 – (a) Original field layout for a 120 MW_{th} Gemasolar-like SPT. (b) Field layout for a 120 MW_{th} variable velocity SPT, where the grey points depict the heliostats eliminated from the field. Both figures show the efficiency of each heliostat at 11 hours of the Spring Equinox with the corresponding optimum aiming strategy selected.

4.2. Thermal analysis

The optimum configuration of the VVR during the Spring Equinox is shown in Table 2 by means of arrows.

Table 2 – Daily configuration of the VVR in the Spring Equinox with a solar field 12.5% smaller than the original one.

	Np (West)	Np (East)	*k*
7h	18 passes 	18 passes 	3
8h	9 passes 	10 passes 	2.5
9h	9 passes 	10 passes 	2
10h	9 passes 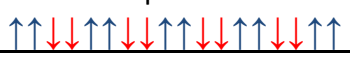	10 passes 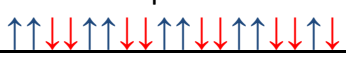	2
11h	9 passes 	10 passes 	2
12h	10 passes 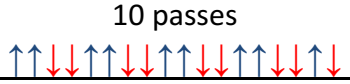	10 passes 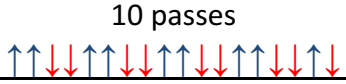	2

292

293 Figure 5 is organized in rows and columns. Each row represents the results for different solar
294 times from 7 h to 12 h in the morning. Each column represents the flux density distribution
295 using the maximum aiming factor afforded by the mechanical and thermal limitations of the
296 material, and the appropriate evolution of the film temperature in the two flow paths,
297 corresponding to the TETR (columns 1 and 2) and the VVR (columns 3 and 4). The film
298 temperature evolution corresponds to the representative tube of each panel. In the TETR nine
299 passes per path have been represented, while for the VVR the number of passes per path
300 varies from 9 to 18 depending on the solar hour.

301 It can be observed that only at 7 h the aiming strategy is equatorial, and then the incident solar
302 flux is higher in the TETR than in the VVR. As the proposed receiver has twice number of
303 passes, its global heat transfer coefficient, for the same mass flow rate, is higher. Therefore,
304 despite of the smaller size of the solar field, the thermal power absorbed by the HTF, at that
305 hour, is similar in both receivers, see Figure 6. A 36-passes receiver configuration is possible
306 due to the low quantity of HTF flowing through the receiver in the early morning, which keeps
307 the pressure drop low enough. For other hours of the day, in which the mass flow rate is
308 higher, the division of all the panels of the receiver is not feasible.

From 8 to 12 h, instead of doubling the number of passes of the receiver, the smaller number of heliostats in the VVR is balanced by increasing the aiming factor in 0.5 points (at 8, 9 and 12 h) or 1 point (at 10 and 11 h) with respect to the TETR. In these cases, to fulfil the operation condition of the SPT, dividing in two passes the last panel of each flow path is enough.

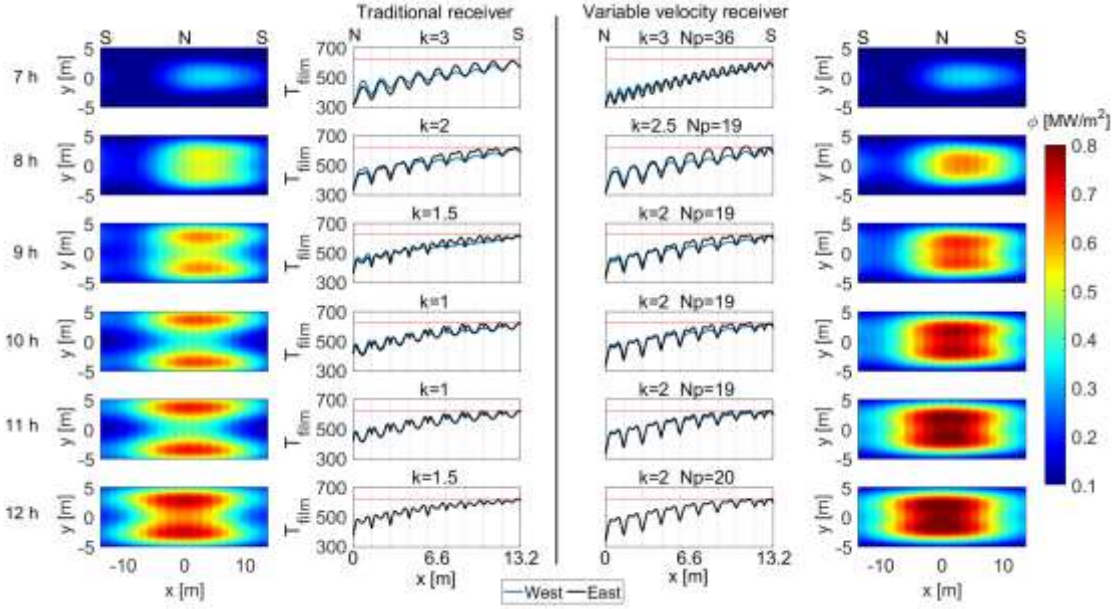

Figure 5 - Flux density distribution and film temperature evolution during the morning of the Spring Equinox (from 7 h to 12 h) for the optimum configurations of the TETR and the VVR. The solid blue line depicts the western flow path, the solid black line the eastern flow path and the solid red line red line the temperature limit that should not be overpassed.

Figure 6.a depicts the field-receiver efficiency of both receivers. The TETR presents the best thermal behaviour at solar noon, when the maximum solar flux density is located at the inlet of the HTF [6]. However, in the VVR the best thermal behaviour is extended to the central hours of the day. The continuity in the efficiency and in the aiming factor selection reduces the control requirement in the solar field.

Near sunrise, sunset and at solar noon the efficiency values in both receivers are quite similar. Nevertheless, two hours before and after solar noon, the VVR presents better results, with a

maximum improvement with respect to TETR of 0.45%. Figure 6.b. shows the daily thermal power absorbed by both receivers. In the first hours after sunrise the TETR absorbs more energy than the VVR, because of the higher solar field size. But close to solar noon the thermal behaviour is just opposite, due to the HTF temperature limitation. The average mass flow rates in the TETR and the VVRs are respectively 154.76 and 157.64 kg/s; this small difference turns into an increment of the thermal energy in the VVR of around 1 MW_{th}, which compensates the increment of the power consumption of the molten salt pumps with regard to the TETR, because of the higher pressure drop.

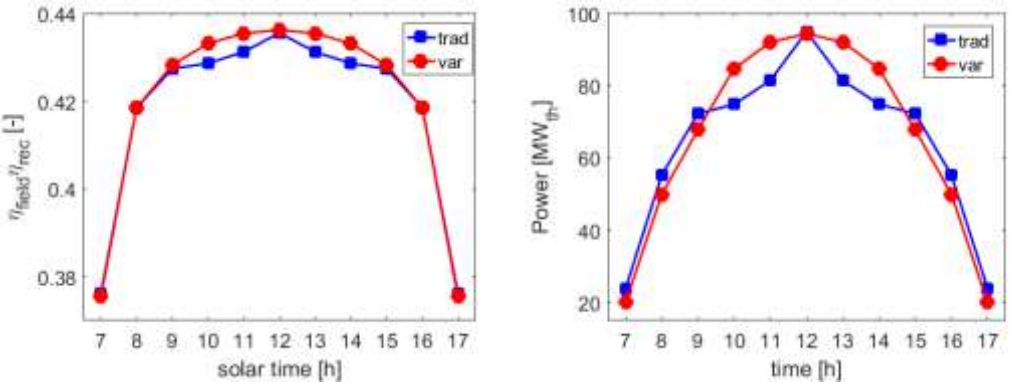

(a) (b)

Figure 6 – (a) Hourly field-receiver efficiency during the Spring Equinox for the TETR and the VVR of 120 MW_{th}. (b) Hourly thermal power absorbed during the Spring Equinox for the TETR and the VVR of 120 MW_{th}.

4.3. Mechanical and hydrodynamic analysis

It has been shown that the improvement, in terms of absorbed thermal energy, with respect to the solar field size in the VVR is considerable. However, there are several mechanical and hydrodynamic disadvantages that must be carefully studied.

On one hand, as the aiming factor increases in the VVR, the peak flux raises causing higher mechanical stresses, as can be seen in Figure 7. Figure 7.a shows the maximum mechanical

stresses of the different panels of the TETR and the VVR at solar noon. It can be seen that the major problems can be found in the first panel of the receiver where the salt is cold and the flux density is the highest. However, thanks to the elimination of northern heliostats in the VVR, the minimum difference between both receivers is found in this first panel.

Independently of the hour, the maximum stress is always located at the first panel. Then, attending to the first panel of each receiver, the maximum hourly mechanical stresses during the Spring Equinox has been shown in Figure 7.b. The mechanical stresses are higher in the central hours of the day, due to the higher flux density. In the new receiver, the mechanical stress increases up to 88 MPa, being around 5 MPa higher than in the TETR. However, as can be seen in Figure 7.c it is still far from the limiting UTS (black solid line), which in average has a value of 580 MPa. Therefore, although the risk of cracking does not increases in the new VVR, special attention has to be paid to fatigue, above all in the first panels of each flow path. To reduce the risk of failure in both receivers, it is recommended to exchange the northern panels by the southern panels during maintenance stops.

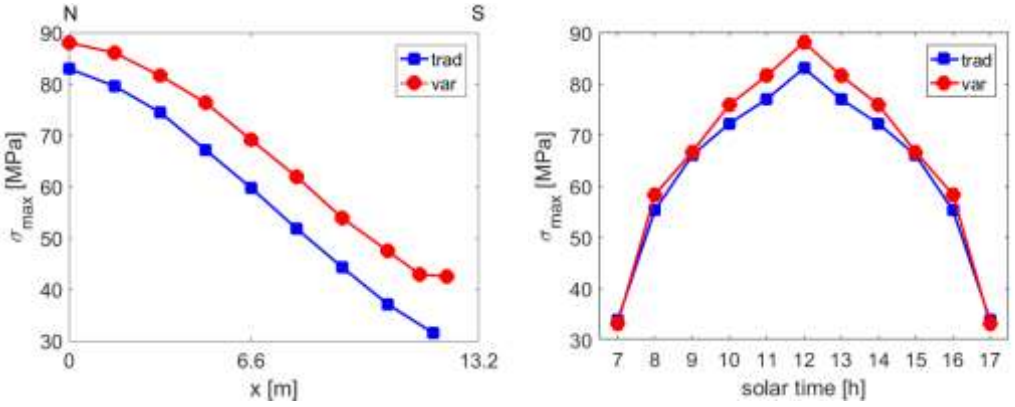

(a) (b)

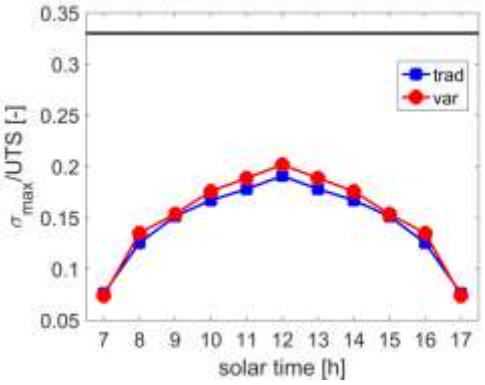

(c)

Figure 7 – (a) Maximum mechanical stresses in the different panels of the TETR and the VVR at solar noon. (b) Maximum hourly mechanical stress and (c) Maximum hourly mechanical stress-UTS ratio for the TETR and the VVR of 120 MW_{th} during the Spring Equinox, where the black line depicts the maximum allowable value.

On the other hand, when the number of passes increases, the HTF travel distance also increases. In the VVR the increment of the number of passes causes higher local velocities of the HTF. Besides, higher aiming factors require higher mass flow rates to cool down the tubes, increasing even more the velocity of the HTF. Therefore, in the VVR there is an increment of pressure drop and parasitic power consumption of the molten salt pumps. Nonetheless, in the worst case, when the mass flow rate is increased, the optimum VVR has only two extra passes with respect to the TETR. In this case, the maximum pressure drop rises from 12 to 28 bars, see Figure 8.a.

Regarding the molten salt pump system, it has been assumed that a variable frequency drive keeps the mechanical efficiency of the pumps almost constant. Hence, the power consumed increases only with the mass flow rate and the pressure drop increment. Assuming an efficiency of the power block of 39.4% [32] and using the operational characteristics of the vertical pump GVSO of Friatec [33], the electric power consumed by: the pump system, P_{pump},

has been calculated (see Equations 12 and 13). Note that H_{pump} represents the head of the pump, which is defined by the height of the tower, the absolute pressure of the storage tanks, p_{tank} = 10^5 Pa, and the pressure drop in the receiver.

$$P_{pump} = \frac{\dot{m}_{salt} H_{pump}}{\varphi \eta_{pump}} \tag{12}$$

$$H_{pump} = \varphi g \Delta h + \Delta p + p_{tank} \tag{13}$$

Figure 8.b compares the parasitic power consumption of both SPT analysed. It can be seen that at first/last hour of the day, the parasitic consumption is quite similar, although the VVR works with higher number of passes. At central hours of the day, this difference raises up to 0.27 MW_e, being the maximum parasitic power consumption of the VVR 0.83 MW_e. As the VVR absorbs 1 $MW_{th} \simeq 0.394 MW_e$ more thermal power than the TETR, there is yet a security factor that ensures the generation capacity of the new SPT.

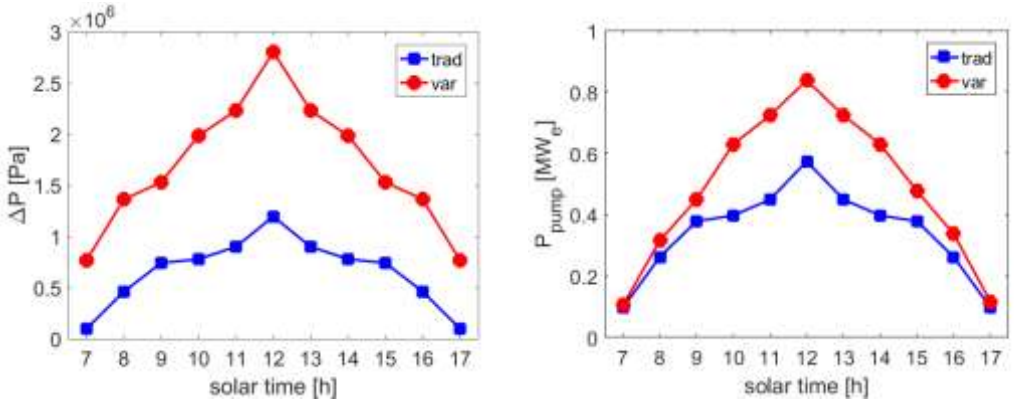

(a) (b)

Figure 8 – (a) Hourly pressure drop in the TETR and the VVR of 120 MW_{th} at solar noon of the Spring Equinox. (b) Hourly mechanical power consumed by the molten salt pumps during the Spring Equinox, for the TETR and the VVR of 120 MW_{th}.

The removal of heliostats in the field may concern during the winter season; a smaller number of heliostats could reduce the mean flux density intercepted by the receiver, diminishing the operational hours of the receiver and the annual generation capacity of the SPT. However, VVRs with smaller number of heliostats have advantages over the TETR. For example, in the case of Winter Solstice the TETR cannot start up until 9 h, when the incident solar flux is high enough to reach turbulent flow of the HTF. Nevertheless, the VVR can start up at 8 h by means of doubling the number of passes in the receiver, so that turbulent flow is reached earlier.

5. Conclusions

The study of the proposed VVR has evidenced several advantages with respect to the TETR with fixed configuration. VVR presents advantages in comparison to receivers with high number of panels, due to smaller pressure drop. But also, this novel receiver presents advantages with respect to receivers with low number of panels, because it reduces the maximum wall temperature responsible of stress corrosion cracking.

Another noticeable advantage of the proposed receiver is the increase of the operational hours when the solar irradiation is low and the Reynolds number of the HTF, in the TETR, is not high enough to reach turbulent regime. In this case, is mandatory to double the number of passes in the VVR. Besides, the VVR allows using more concentrated aiming strategies, which reduces the spillage losses and increases the efficiency of the SPT. In addition to this, the presented receiver simplifies the control of the solar field.

For the specific case studied, Spring Equinox in a 120 MW_{th} Gemasolar-like SPT, the net generation capacity is kept constant with a solar field size reduction of 12.5% (331 heliostats). In the proposed VVR, the efficiency is enhanced by means of higher optical efficiency of the field and higher HTF velocities in some specific parts of the receiver, which allows reducing the tube wall temperature. The inconvenient of this new receiver is the slight increment of the mechanical stresses in the receiver, from 83 to 88.1 MPa. Although, the mechanical stress is

still far of the material operational limit it could increase the fatigue. However, it can be solved by exchanging the northern panels by the southern panels of the receiver during maintenance stops.

Acknowledgments

This work has been supported by the Spanish government under the projects ENE2012-34255 and ENE2015-69486-R.

References

[1] V. Ruiz, M. Frasquet, F. Martínez, M. Silva, I. Lillo, F.D. Andrades, et al., The Variable Geometry Central Receiver System Concept. First Results and Comparison with Conventional Central Receiver Systems, Energy Procedia. 57 (2014) 2255–2264. doi:10.1016/j.egypro.2014.10.233.

[2] S. Hübner, M. Eck, C. Stiller, M. Seitz, Techno-economic heat transfer optimization of large scale latent heat energy storage systems in solar thermal power plants, Appl. Therm. Eng. 98 (2016) 483–491. doi:10.1016/j.applthermaleng.2015.11.026.

[3] T.W. Neises, M.J. Wagner, A.K. Gray, Structural Design Considerations for Tubular Power Tower Receivers Operating at 650 ° C Preprint, 2014.

[4] M. Shiva Prasad, K. Chandra Sekhar Reddy, S. Sakthivel, Development of cost efficient solar receiver tube with a novel tandem absorber system, Appl. Therm. Eng. (2016). doi:10.1016/j.applthermaleng.2016.05.163.

[5] N. Boerema, G. Morrison, R. Taylor, G. Rosengarten, Liquid sodium versus Hitec as a heat transfer fluid in solar thermal central receiver systems, Sol. Energy. 86 (2012) 2293–2305. doi:10.1016/j.solener.2012.05.001.

[6] M.R. Rodríguez-Sánchez, A. Sánchez-González, C. Marugan-Cruz, D. Santana, Flow

443 patterns of external solar receivers, Sol. Energy. 122 (2015) 940–953.
444 doi:10.1016/j.solener.2015.10.025.

445 [7] O. Garbrecht, F. Al-Sibai, R. Kneer, K. Wieghardt, CFD-simulation of a new receiver
446 design for a molten salt solar power tower, Sol. Energy. 90 (2013) 94–106.
447 doi:10.1016/j.solener.2012.12.007.

448 [8] M.R. Rodríguez-Sánchez, A. Sánchez-González, C. Marugán-Cruz, D. Santana, New
449 Designs of Molten-salt Tubular-receiver for Solar Power Tower, Energy Procedia. 49
450 (2014) 504–513. doi:10.1016/j.egypro.2014.03.054.

451 [9] N. Boerema, G. Morrison, R. Taylor, G. Rosengarten, High temperature solar thermal
452 central-receiver billboard design, Sol. Energy. 97 (2013) 356–368.
453 doi:10.1016/j.solener.2013.09.008.

454 [10] P.J. Turner, C. Sansom, A Tubed, Volumetric Cavity Receiver Concept for High
455 Efficiency, Low-cost Modular Molten Salt Solar Towers, Energy Procedia. 69 (2015) 553–
456 562. doi:10.1016/j.egypro.2015.03.064.

457 [11] L. Yang, R. Zhou, X. Jin, X. Ling, H. Peng, Experimental investigate on thermal properties
458 of a novel high temperature flat heat pipe receiver in solar power tower plant, Appl.
459 Therm. Eng. 109 (2016) 610–618. doi:10.1016/j.applthermaleng.2016.07.075.

460 [12] M.R. Rodríguez-Sánchez, A. Sánchez-González, A. Acosta-Iborra, D. Santana, Variable
461 Velocity in Solar External Receivers, in: SolarPACES, Abu Dhabi, 2016: pp. 1–8.

462 [13] M.R. Rodríguez-Sánchez, A. Soria-Verdugo, J.A. Almendros-Ibáñez, A. Acosta-Iborra, D.
463 Santana, Thermal design guidelines of solar power towers, Appl. Therm. Eng. 63 (2014)
464 428–438. doi:10.1016/j.applthermaleng.2013.11.014.

465 [14] A.K. Das, P. Iñigo, R.J. Terdalkar, A. Joshi, C. Wang, M.M. Clark, et al., Design Features

and Control Concepts of ALSTOM Molten Salt Receiver, Energy Procedia. 69 (2015) 350–359. doi:10.1016/j.egypro.2015.03.040.

[15] A. Sánchez-González, D. Santana, Solar flux distribution on central receivers: a projection method from analytic function., Renew. Energy. 74 (2015) 576–587.

[16] H.C. Hottel, A simple model for estimating the transmittance of direct solar radiation through clear atmospheres, Sol. Energy. 18 (1976) 129–134. doi:10.1016/0038-092X(76)90045-1.

[17] F.J. Collado, A. Gómez, J.A. Turégano, An analytic function for the flux density due to sunlight reflected from a heliostat.pdf, Sol. Energy. 37 (1986) 215–34.

[18] P.L. Leary, J.D. Hankins, User's guide for MIRVAL: a computer code for comparing designs of heliostat-receiver optics for central receiver solar power plants., 1979.

[19] F.J. Collado, DESIGN OF SOLAR TOWER PLANTS HELIOSTAT BY HELIOSTAT : THE SHADOWING AND BLOCKING FACTOR, in: SolarPACES, Granada, Spain, 2011: pp. 1–8.

[20] A.B. Zavoico, Solar Power Tower: Design Basis Document, San Francisco, SAND2001-2100, 2001.

[21] J.E. Pacheco, Final Test and Evaluation Results from the Solar Two Project, Albuquerque, SAND2002-0120, 2002.

[22] M.R. Rodríguez-Sánchez, A. Sánchez-González, D. Santana, Revised receiver efficiency of molten-salt power towers, Renew. Sustain. Energy Rev. 52 (2015) 1331–1339. doi:10.1016/j.rser.2015.08.004.

[23] M.R. Rodríguez-Sánchez, C. Marugan-Cruz, A. Acosta-Iborra, D. Santana, Comparison of simplified heat transfer models and CFD simulations for molten salt external receiver, Appl. Therm. Eng. 73 (2014) 991–1003. doi:10.1016/j.applthermaleng.2014.08.072.

489 [24] F.M. Modest, Radiative Heat Transfer, in: Radiat. Heat Transf., Second Edi, Elsevier
490 science, New York, San Francisco, London, 2003: pp. 162–197.

491 [25] I.E. Idelchik, Handbook of Hydraulic Resistance, third, Begell House, New York, USA,
492 1986.

493 [26] O. Flores, C. Marugán-Cruz, D. Santana, M. García-Villalba, Thermal Stresses Analysis of
494 a Circular Tube in a Central Receiver, Energy Procedia. 49 (2014) 354–362.
495 doi:10.1016/j.egypro.2014.03.038.

496 [27] C. Marugán-Cruz, O. Flores, D. Santana, M. García-Villalba, Heat transfer and thermal
497 stresses in a circular tube with a non-uniform heat flux, Int. J. Heat Mass Transf. 96
498 (2016) 256–266. doi:10.1016/j.ijheatmasstransfer.2016.01.035.

499 [28] ASME, ASME Boiler and Pressure Vessel Code, Section II - Materials, American Society
500 of Mechanical Engineers, New York, 2011.

501 [29] R.W. Bradshaw, Thermal Convection Loop Study of the Corrosion of Incoloy 800 (1) in
502 Molten " E, Corrosion-Nace. 43 (1987) 173–178.

503 [30] A. Sánchez-González, M.R. Rodríguez-Sánchez, D. Santana, Aiming strategy model
504 based on allowable flux densities for molten salt central receivers, Sol. Energy. (2016).
505 doi:10.1016/j.solener.2015.12.055.

506 [31] G.J. Kolb, S.A. Jones, M.W. Donnelly, D. Gorman, R. Thomas, R. Davenport, et al.,
507 Heliostat Cost Reduction Study, Albuquerque, SAND2007-3293, 2007.

508 [32] T. Sano, Development of the Ultra High Efficiency Thermal Power Generation Facility,
509 in: India Energy Congr., 2009: pp. 1–11.

510 [33] M.R. Rodriguez-Sanchez, A. Sanchez-Gonzalez, C. Marugan-Cruz, D. Santana, Saving
511 assessment using the PERS in solar power towers, Energy Convers. Manag. 87 (2014)

512 810–819. doi:10.1016/j.enconman.2014.07.076.

513